The electronic structures of BEDT-TTF·PF_6 crystals; a comparison of self-consistent field and Hubbard model analyses

Ping Tang, N. A. W. Holzwarth,* and Freddie R. Salsbury, Jr.
Department of Physics, Wake Forest University, Winston-Salem, NC 27109-7507

Jeremy Qualls
Department of Physics and Geology, University of Texas Pan American, Edinburg, TX 78539
(Dated: October 7, 2004)

There has been considerable experimental and theoretical interest in synthetic materials formed from charge transfer salts of BEDT-TTF (bis-ethylenedithio-tetrathiafulvalene). Three crystalline forms of (BEDT-TTF)·PF_6 have been identified experimentally,[1–3] and labeled δ, ϵ, and ζ. We have modeled these three materials using first-principles self-consistent field methods, to determine the optimal geometrical parameters, the densities of state, and electron density contour plots for states near the Fermi level. The ϵ and ζ crystals are found to be metallic, while the δ crystals, with twice as many molecules per unit cell, are found to be insulating. By contrast, experimental conductivity and optical measurements for the ζ material[3] suggest a Mott insulator behavior. We examine the Hubbard model for this system to understand both the Mott insulating behavior and the failure of the self-consistent field methods to model it.

I. INTRODUCTION

The study of synthetic crystalline materials based on charge transfer salts formed from organic donor molecules and a variety of acceptor complexes has been an active area of research for the past 30 years.[4,5] While an important motivation for much of this work is due to superconducting properties, a rich variety of other interesting phenomena are exhibited in these materials.[6]

The donor molecule bis-ethylenedithio-tetrathiafulvalene, abbreviated as BEDT-TTF or ET, has been used to make more than 100 different charge transfer crystals.[4] In the present work, we study three materials which have been characterized with the stoichiometry (BEDT-TTF)·PF_6. In these materials, the donor BEDT-TTF molecules has a formal charge of $+1$ while the acceptor complex (PF_6) has a formal charge of -1. Three crystalline forms of (BEDT-TTF)·PF_6 have been identified experimentally, and labeled δ[1], ϵ[2], and ζ.[3] The electronic properties have been characterized for the ζ form[3] which was found to be semiconducting with a band gap of approximately 0.5 eV. Our calculational results provide a framework for comparing the structural and electronic properties of the three materials relative to each other and relative to other similar materials.

Apart from the references cited above, there has been rather little work done on the (BEDT-TTF)·PF_6 materials. However, there is a very large literature of work on other BEDT-TTF materials, including several forms of $(BEDT\text{-}TTF)_2\cdot PF_6$. Most of these materials have a stoichiometry of two BEDT-TTF molecules for each accepter complex, so that each BEDT-TTF molecule has a formal charge of $+1/2$.

Although, to our knowledge, there has been no previous theoretical work on the (BEDT-TTF)·PF_6 materials, there have been a number theoretical studies of other BEDT-TTF materials. Due to the complexity of these materials, there are relatively few[7,8] first-principles calculations for the full crystals although there have been a number of first-principles studies of the BEDT-TTF molecule in different charge states.[9–14]

The outline of this paper is as follows. Section II describes the crystal structures and the molecular configurations for the three materials, including a comparison of measured and calculated bond lengths. Section III describes the local density approximation analyses of the electronic structure of the three crystal structures, including their densities of states, band diagrams, charge density contours for states near the Fermi level, and a tight-binding fit of the Fermi level bands. The Hubbard model analysis is presented in Section IV, including both a discussion of the infinite half-filled one-dimensional case and a more detailed analysis of the two electron dimer. The results of quantum chemical treatments of molecular dimers of this system are presented in Section V and related to the Hubbard dimer analysis. A summary of the results and conclusions are presented in Section VI.

II. CRYSTAL STRUCTURES

Lattice parameters from X-ray analyses[1–3] are summarized in Table I for the three crystalline forms of (BEDT-TTF)·PF_6: δ, ϵ, and ζ. The ϵ and ζ structures both contain one formula unit per primitive cell, while the δ structure contains two formula units and therefore has roughly twice the primitive cell volume. The δ and ζ structures have a single symmetry element – inversion, while the ϵ structure has 4 symmetry elements including inversion and a mirror plane or equivalently a two-fold rotation and mirror plane.

The structure of the $BEDT\text{-}TTF^+$ molecular ion is shown in Fig. 1, with atoms labels using the same convention as Williams and coworkers.[15,16] The main portion of $BEDT\text{-}TTF^+$ ion is nearly planar (even more so than the neutral molecule as shown in Fig. 2 below), which

TABLE I: Lattice parameters for BEDT-TTF)·PF_6 crystals determined from X-crystallography.

	δ^a	ϵ^b	ζ^c
Symmetry	P$\bar{1}$	C2/m	P$\bar{1}$
a (Å)	6.4253	14.5270	6.2293
b (Å)	10.7241	10.7350	7.2633
c (Å)	13.049	5.9233	9.8662
α (deg)	84.084	90.000	93.898
β (deg)	82.435	105.559	93.592
γ (deg)	87.378	90.000	97.914
Volume (Å^3)	886.1	444.9	439.95

[a]Ref. 1, presumed to be room temperature.
[b]Ref. 2, presumed to be at room temperature. The quoted lattice constants represent the conventional unit cell, while the volume is that of the primitive cell.
[c]Ref. 3 at T=173 K.

is described in the $\hat{\mathbf{x}} - \hat{\mathbf{y}}$ plane with $\hat{\mathbf{x}}$ pointing along the long molecular axis as defined by the C2−C1 bond. The drawing shows the structure appropriate for the ϵ material with four-fold 2/m symmetry about the center of the molecule. The structure of the BEDT-TTF^+ ion appropriate for the δ and ζ materials has only inversion symmetry about the center and differs primarily in the arrangement of the end carbon and hydrogen groups; so that the C7−C8 and C9−C10 bonds are no longer parallel to the $\hat{\mathbf{y}}$ axis.

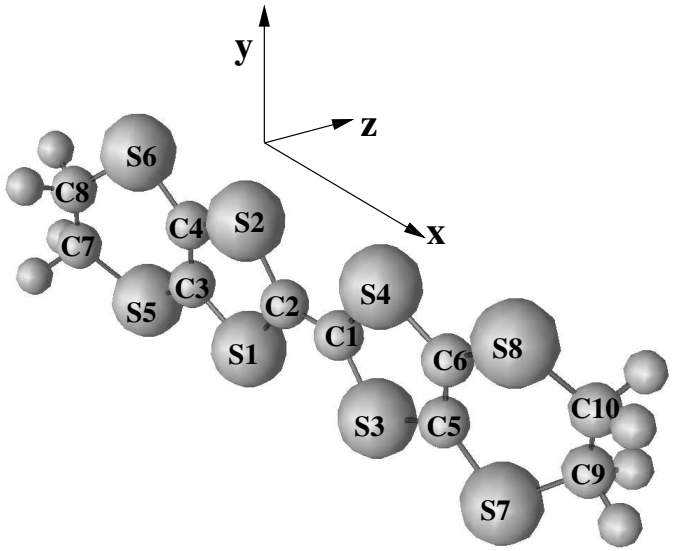

FIG. 1: Ball and stick diagram of a BEDT-TTF+ molecule[16] defining local coordinate system and atomic labels for carbon (C) and sulfur (S) sites. The hydrogen sites are not labeled.

In addition to the local symmetry of each BEDT-TTF^+ molecule, an important characteristic of the crystal is the arrangement or stacking of the molecules within the structure.[17] In order to quantify this stacking, it is helpful to express the nearest molecule displacements, referenced to the molecule centers, and using the coordinate system defined in Fig. 1. Some of the nearest neighbor displacements

$$\mathbf{R} = X\hat{\mathbf{x}} + Y\hat{\mathbf{y}} + Z\hat{\mathbf{z}}, \tag{1}$$

of the BEDT-TTF^+ molecules in each of the crystals are calculated from the X-ray results[1–3] and listed in Table II. The δ structure has the smallest R corresponding to its two BEDT-TTF^+ ions in its primitive cell in a parallel stacking arrangement. In this case the molecular planes are separated by 3.47 Å along the Z axis while the molecular centers are shifted by 3.14 Å (approximately one pentagonal ring) along the X axis. The next nearest neighbor stacking is primarily along the vertical Y axis due to the lattice translation **a**. By virtue of the fact that there is a single BEDT-TTF^+ per primitive unit cell for the ϵ and ζ structures, the molecular ions stack in parallel planes. In the ϵ structure, a nearest neighbor stacking similar to that of the δ structure is achieved with the translation vector along its **c** axis with a separation of 3.48 Å along the Z axis and a shift of the molecular centers of 4.79 Å along the X axis. For the ζ structure, the nearest neighbor stacking is achieved by the translation vector along its **a** axis, causing a vertical displacement along the Y axis by 5.46 Å with a plane separation of 2.44 Å along the Z axis and a smaller shift along the X axis. In addition, the translation vector along its **b** axis, listed as the second entry in the table, also may contribute significant intermolecular interactions.

TABLE II: Displacements (Eq. 1) of nearest neighbor BEDT-TTF^+ ions expressed in terms of the distance R between molecular centers and the corresponding X,Y, and Z components in the local coordinate system shown in Fig. 1. All values are taken form the crystallographic data[1–3] and are listed for $R \leq 9$ Å. When appropriate, the corresponding lattice translation vector is listed in the second column.

Crystal Structure	lattice translation	R	X	Y	Z
δ		4.88	3.14	0.16	−3.47
	a	6.43	1.52	5.92	1.91
ϵ	**c**	5.92	4.79	0.00	3.48
ζ	**a**	6.23	−1.75	5.46	−2.44
	b	7.26	6.07	−0.93	−3.88

Some of the molecular bond lengths for the three crystals are listed in Table III, comparing values derived from X-ray measurements with those derived from the calculations presented in this paper. Interestingly, the table shows remarkable agreement, within ±0.03 Å in the C−C and C−S bond lengths for the three structures and for experimental and calculated values. One notable exception is the measured value of the C7−C8 bond length for the ϵ structure which, perhaps due to noise, was reported to be unphysically small for an expected single bond carbon group. The unrestricted Hartree-Fock

TABLE III: Some bond lengths (in units of Å) for (BEDT-TTF)·PF_6 crystals, comparing experimental ("EXP") with calculated values both using local density approximation ("LDA") on the crystals and unrestricted Hartree-Fock ("UHF") on the BEDT-TTF^+ molecular ion, as described below. For the lower symmetry δ and ζ structures, the entry represents an average over similar bond lengths.

	δ		ϵ			ζ		
Bond	EXP[a]	LDA	EXP[b]	LDA	UHF	EXP[c]	LDA	UHF
C1-C2	1.38	1.39	1.40	1.37	1.39	1.38	1.39	1.39
C3-C4	1.35	1.37	1.35	1.37	1.34	1.36	1.37	1.34
C7-C8	1.50	1.51	1.32	1.52	1.54	1.51	1.50	1.52
C2-S2	1.72	1.74	1.71	1.74	1.73	1.73	1.74	1.72
C4-S2	1.72	1.74	1.74	1.75	1.74	1.74	1.75	1.75
C4-S6	1.74	1.74	1.73	1.73	1.75	1.75	1.75	1.76
C8-S6	1.81	1.82	1.77	1.82	1.83	1.81	1.82	1.82

[a]Ref. 1
[b]Ref. 2
[c]Ref. 3

(UHF) results for the BEDT-TTF^+ molecular ions reported here are consistent with the earlier work of Demiralp and Goddard.[9] Figure 2 shows an edge view of the UHF optimized molecular structures showing the symmetry difference between the ϵ and ζ forms and showing the high degree of planarity of the ionic forms.

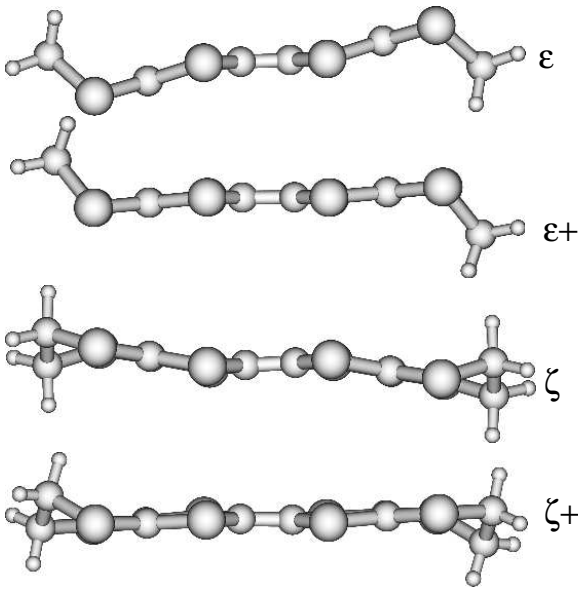

FIG. 2: Edge view of neutral and ionic molecular structures for the BEDT-TTF molecules, calculated as discussed in Section V.

As a part of the optimization calculations, we can estimate the stability of the 3 crystalline forms. The *pwpaw* calculations for the three crystals described in Section III suggest that the order of stability is $\zeta > \delta > \epsilon$, with larger error bars on the δ structure results. The quantum chemical studies described in Section V suggest that the lower symmetry ζ form is more stable than the ϵ form for the BEDT-TTF^+ molecular ions themselves, which should contribute to the stability of corresponding crystals.

III. LDA ELECTRONIC STRUCTURES

A. Calculational details

The calculations in this section were done within the framework of density functional theory and the local density approximation (LDA)[18,19] using the exchange-correlation functional of Perdew and Wang,[20] assuming all occupied Bloch states to have equal numbers of spin up and spin down electrons.

The LDA calculations were carried out with a plane-wave basis representation using the projector augmented wave formalism of Blöchl[21] with the *pwpaw* code.[22] The necessary projector and basis functions were generated with the atompaw code[23] using the parameters listed in Table IV. With this parameter set the plane wave cut-offs could be chosen as 10 bohr^{-1} and 12 bohr^{-1} for the wavefunction and density planewave expansions, respectively. The Brillouin zone integrals were approximated by 1, 6, and 9 **k**-point samplings for the δ, ϵ, and ζ structures, respectively in order to calculate the density of states. The geometry optimizations, which are less sensitive to the Brillouin zone sampling, were performed with single **k**-point sampling point. The results of these optimization calculations are listed in Table III.

Three-dimensional graphics (Figs. 1 and 7) were generated using OpenDX.[24]

TABLE IV: Atomic numbers (Z), basis function quantum numbers (nl), and augmentation radii (r_c^a) used to construct basis and projector functions.

Atom	Z	nl basis	r_c^a (bohr)
H	1	$1s$	0.710
C	6	$2s\ 2p$	1.010
F	9	$2s\ 2p$	1.145
P	15	$3s\ 3p\ \epsilon d$	1.710
S	16	$3s\ 3p\ \epsilon d$	1.810

B. Densities of states

The partial densities of states $N^a(E)$, weighted by the charge contained in a sphere about the atom a, was calculated using a Gaussian smearing function[25,26] in the following form:

$$N^a(E) = \frac{2}{\sqrt{\pi}\sigma} \sum_{n\mathbf{k}} C^a_{n\mathbf{k}}\ W_{\mathbf{k}}\ \mathrm{e}^{-(E-E_{n\mathbf{k}})^2/\sigma^2}. \quad (2)$$

Here the factor of 2 comes from assuming double occupancy for each state denoted with band index n and

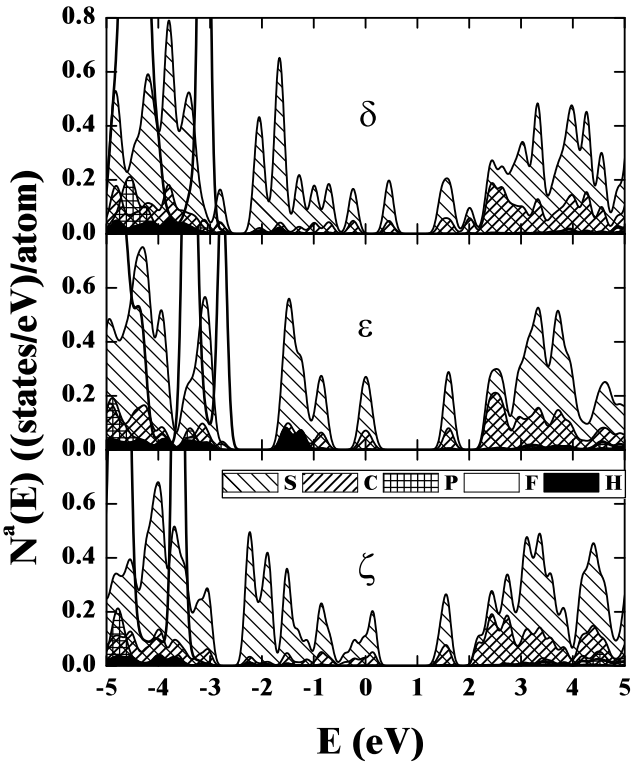

FIG. 3: Partial densities of states for δ, ϵ, and ζ forms of BEDT-TTF·PF_6 in their experimentally determined crystal structures, showing contributions from spheres surrounding S, C, H, P, and F sites. The energy scale is zeroed at the Fermi level for each material.

wavevector $\mathbf{k}$ having band energy $E_{n\mathbf{k}}$. The normalized Brillouin zone weight factors are denoted by $W_{\mathbf{k}}$. The coefficient $C^a_{n\mathbf{k}}$ represents the charge contained in a single sphere enclosing atom a, with radius taken to be the augmentation radii r^a_c listed in Table IV and averaged over inequivalent atoms of the same atomic species. The Gaussian smearing parameter was taken to be $\sigma = 0.12$ eV.

The partial densities of states for the three crystals are shown in Fig. 3 within a range of ± 5 eV of the Fermi level. The results presented are for the crystals in their experimentally determined crystal structure. The corresponding densities of states for the geometrically optimized structures were very similar, differing primarily in the relative locations of states associated with F sites, 2.5 eV or more below the Fermi level.

The states within $\approx \pm$ 2.5 eV of the Fermi level for all three materials are all associated with the BEDT-TTF^+ molecular ions. Because of the coarse Brillouin zone sampling, the detailed shapes of the partial density of states curves are not well-determined, but the general location of the bands and their widths can be recognized. From these results, we find the δ structure to have a band gap at the Fermi level, while for the ϵ and ζ structures the Fermi level falls in the middle of a narrow band having a width of less than 1 eV.

The curves show that partial densities of states for the states near the Fermi level are dominated by S and C contributions. Since the charge within the augmentation spheres was chosen as the weighting factor for the partial density of states defined in Eq. 2, the S contributions are over estimated relative to those of C. As we will see in Section III D, the S and C contributions are very similar near the Fermi level.

C. Band dispersions

We have studied the band dispersions of these materials in the directions of the reciprocal lattice vectors which are referenced to the molecule-centered coordinate system defined in Fig. 1 in Table V. For the ϵ structure, we use the notation $\mathbf{G}_{A'}$ and $\mathbf{G}_{B'}$ to distinguish the primitive lattice vectors from the conventional lattice vectors listed in Table I.

TABLE V: Primitive reciprocal lattice vector magnitudes and directions expressed in the coordinate system defined in Fig. 1. Length $|\mathbf{G}_i|$ is given in units of Å^{-1}; direction is given in terms of unit vector components.

Crystal		$\lvert\mathbf{G}_i\rvert$	$\hat{\mathbf{x}}$	$\hat{\mathbf{y}}$	$\hat{\mathbf{z}}$
δ	$\mathbf{G}_A$	0.98	0.11	0.93	0.35
	$\mathbf{G}_B$	0.59	0.53	-0.38	0.76
	$\mathbf{G}_C$	0.49	0.76	0.02	-0.65
ϵ	$\mathbf{G}_{A'}$	0.74	0.36	0.79	-0.49
	$\mathbf{G}_{B'}$	0.74	0.36	-0.79	-0.49
	$\mathbf{G}_C$	1.10	0.94	0.00	0.35
ζ	$\mathbf{G}_A$	1.02	-0.20	0.83	0.52
	$\mathbf{G}_B$	0.88	0.76	-0.04	0.65
	$\mathbf{G}_C$	0.64	-0.52	-0.48	0.70

The electronic band dispersions of the three materials are presented in Figs. 4, 5, and 6. The bands are very flat, generally having dispersions of a few tenths of an eV. However, the ϵ and ζ crystals have a single more dispersive band that passes through the Fermi level. The δ crystal has two slightly dispersive bands near the Fermi level. In each of these cases, the dispersion is greatest in the direction of the largest reciprocal lattice vector as listed in Table V.

D. Electronic states near the Fermi level

Since the states near the Fermi level are well isolated from the other states of the system and are largely responsible for the interesting electronic and structural properties of these materials we have examined them in greater detail.

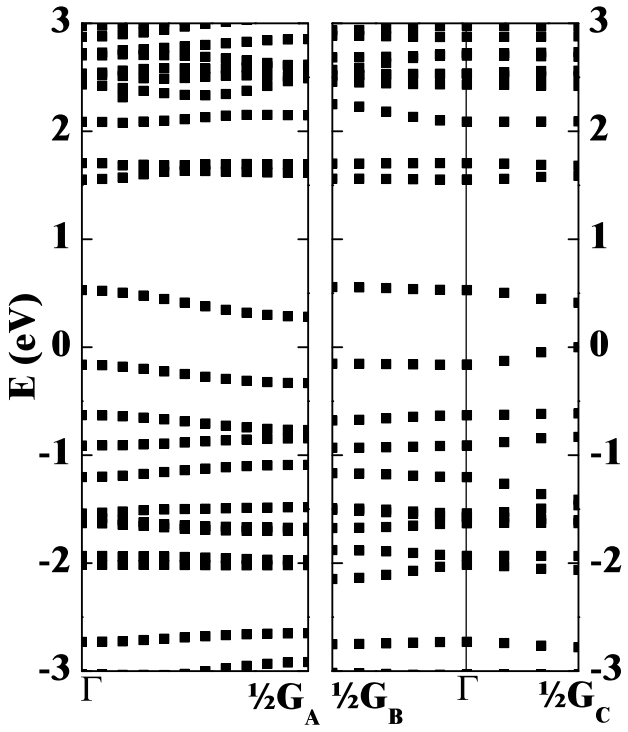

FIG. 4: Band structure of δ BEDT-TTF·PF_6 plotted along the primitive reciprocal lattice vectors.

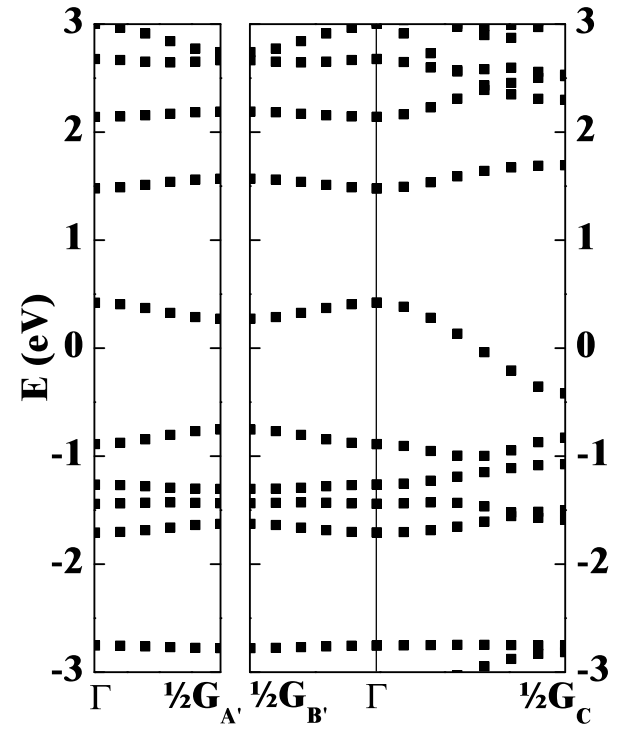

FIG. 5: Band structure of ϵ BEDT-TTF·PF_6 plotted along the primitive reciprocal lattice vectors.

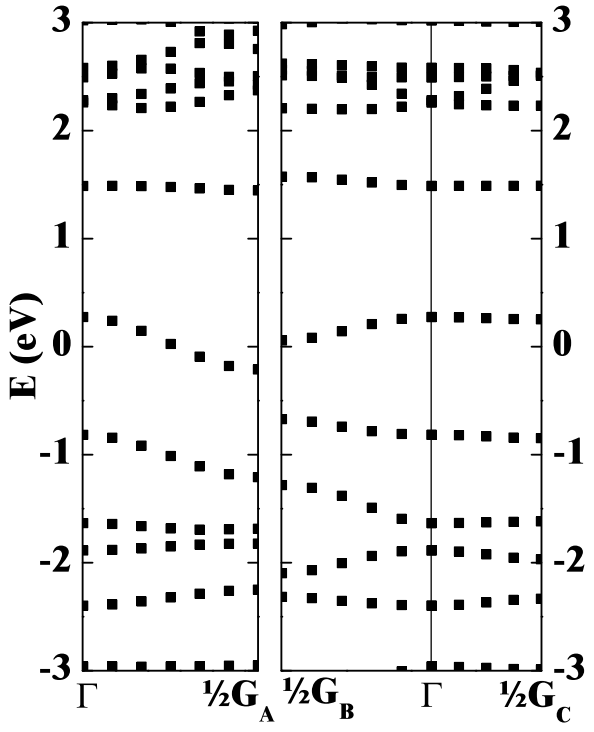

FIG. 6: Band structure of ζ BEDT-TTF·PF_6 plotted along the primitive reciprocal lattice vectors.

1. *Charge density distributions*

We have constructed electronic charge contour maps for the electrons associated with the band closest to the Fermi level for the three materials. These are plotted in several planes in Fig. 7. The results are shown for the structurally optimized forms of the three crystals. What is most interesting in this diagram is the fact that the charge contours are remarkably similar and that for the three crystals, the TTF portions of the BEDT-TTF molecules have the most significant contribution, including π-electron contributions from C double bonds and also from the associated S atoms. Contributions from S atoms in the hexagonal rings are less significant. These charge contours seem to also be consistent with the HOMO (highest occupied molecular orbital) plot presented by Demiralp and Goddard[9] for a neutral BEDT-TTF molecule.

2. *Tight-binding analysis*

In order to examine the band dispersions near the Fermi level in greater detail, we have fit them to a simple tight binding model form. For the δ structure, there are two molecules per primitive cell which are separated by a non-primitive lattice translation $\mathbf{R}$ and therefore the two

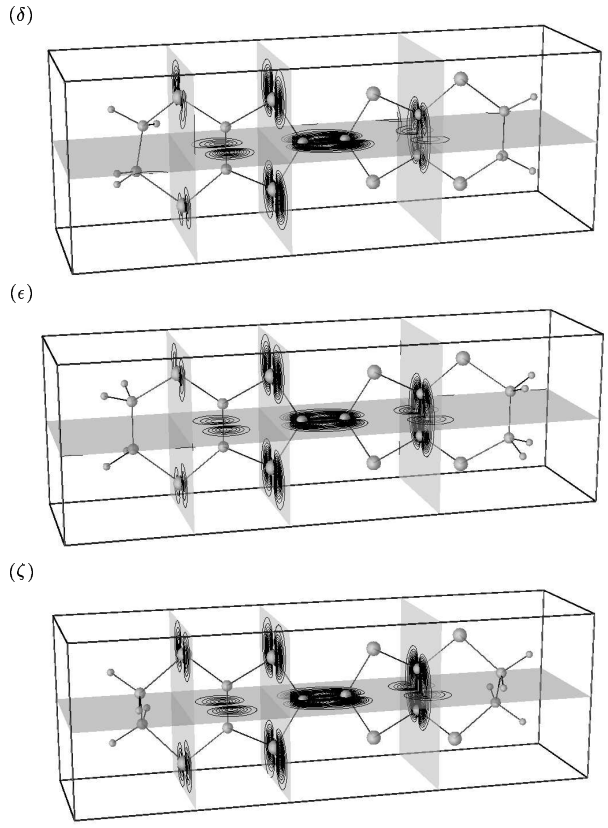

FIG. 7: Contour plot of charge density associated with occupied states near the Fermi level of BEDT-TTF in the δ, ϵ, and ζ structures. Contours are drawn in 4 planes passing through C and S atoms. The contour values are multiples of 0.005 electrons/Å^3.

coupled bands near the Fermi level can be expressed in the form

$$E_{n_\pm}(\mathbf{k}) = U_{11}(\mathbf{k}) \pm U_{12}(\mathbf{k}), \tag{3}$$

where the diagonal functions are given by

$$U_{11}(\mathbf{k}) = \sum_{\mathbf{T}} M_{11}(\mathbf{T}) \cos(\mathbf{k}\cdot\mathbf{T}), \tag{4}$$

and the off diagonal functions are given by

$$U_{12}(\mathbf{k}) = |\sum_{\mathbf{T}} M_{12}(\mathbf{T}) e^{i\mathbf{k}\cdot\mathbf{T}}|. \tag{5}$$

In these expressions, $\mathbf{T} \equiv n_a\mathbf{a} + n_b\mathbf{b} + n_c\mathbf{c}$ represents a lattice translation vector. The matrix element $M_{11}(\mathbf{T})$ represents a Hamiltonian matrix element between orthogonalized molecular states on equivalent BEDT-TTF molecules separated by $\mathbf{T}$. The off-diagonal matrix element $M_{12}(\mathbf{T})$ represents a Hamiltonian matrix element between orthogonalized molecular states on inequivalent BEDT-TTF molecules separated by $\mathbf{R}+\mathbf{T}$. For the ϵ and ζ structures there is only a single molecule in each unit cell so that, so that the dispersion of the band (n_0)

TABLE VI: Tight binding matrix elements (in units of eV) for bands near Fermi level of BEDT-TTF·PF_6 in the δ, ϵ, and ζ. The constant matrix elements $M_{11}(\mathbf{0})$ have been adjusted to represent the same zero of energy as in the partial density of states and band structure plots.

δ			ϵ		ζ	
T	M_{11}	M_{12}	**T**	M_{11}	**T**	M_{11}
0	0.11		**0**	-0.02	**0**	0.00
a	0.11		**c**	0.31	**a**	0.24
0		0.26	**a′,b′**	0.03	**b**	0.10
c		0.06	**a′+c,b′+c**	0.06	**a+b**	0.00
a		0.02	**a′-b′**	0.00	**c**	-0.05
			a′-c,b′-c	-0.01	**a-b**	-0.02
			2c	-0.02		

can be expressed in the simpler form

$$E_{n_0\mathbf{k}} = U_{11}(\mathbf{k}), \tag{6}$$

where $U_{11}(\mathbf{k})$ has the form given in Eq. 4.

The fitting parameters are tabulated in Table VI. These were fit to the band structure results shown in Figs. 4, 5, and 6, calculated from the experimental crystal structures. In order to stabilize the fit, it was necessary to use $\mathbf{k}$ points at general points in the Brillouin zone in addition to the special directions plotted in the band structure diagrams. For each of these fits, the nearest neighbor contribution has a magnitude that is at least twice as large as the next leading term. The density of states curves corresponding to these tight-binding fits are shown in Fig. 8. These were calculated using the Gilat-Raubenheimer method,[27,28] and are very sensitive to the tight binding coefficients $M_{11}(\mathbf{T})$ and $M_{12}(\mathbf{T})$. These results show the band gap of the δ crystal to be 0.2 eV and the band widths of the ϵ and ζ crystals to be 0.8 eV.

E. Criticism of LDA results

While the results presented above make a nice story, they are inconsistent with the experimental measurements reported for the ζ material.[3] In particular, the temperature and dependence of the zero frequency conductivity and optical studies suggest that the material has an electrical band gap of $E_g \approx 0.5$ or 0.6 eV. In addition, the temperature dependence of the magnetic susceptibility suggests that there are low energy spin fluctuations. The authors of Ref. 3 suggest that the ζ crystal behaves like a Mott-Hubbard insulator.

While the LDA approach does an excellent job of approximating the electron response to the lattice and to the mean-field contributed by all the electrons of the system, it under estimates the effects of correlated electron-electron repulsions. In fact, any single particle treatment which assumes equal spin occupancy for each spatial state would predict the ϵ and ζ structures to be metallic by virtue of the fact that they both have an odd number of electrons in their primitive cells.

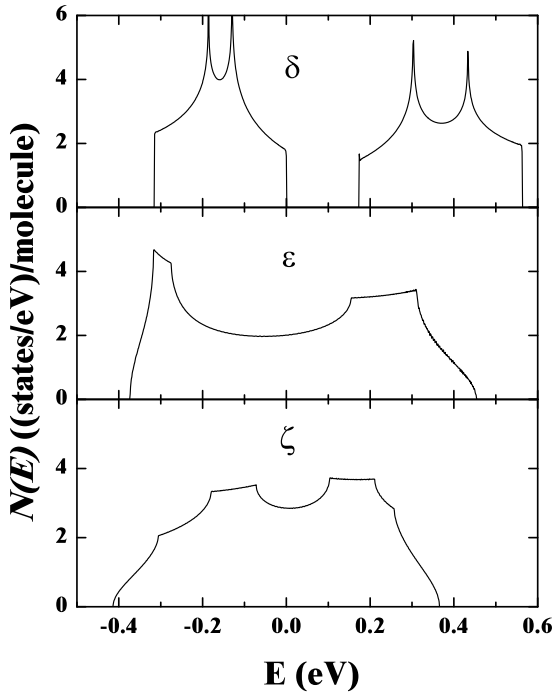

FIG. 8: Density of states for the bands near the Fermi level of the δ, ϵ, and ζ structures.

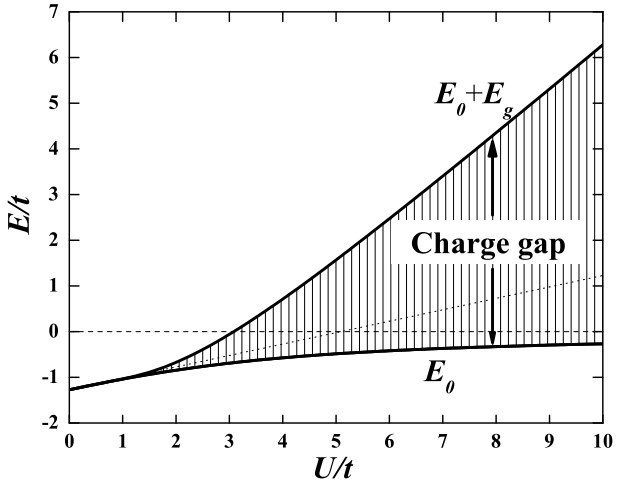

FIG. 9: Plot of the Lieb and Wu[34] solutions for the infinite one-dimensional Hubbard model for the ground state energy E_0 and first excited state accessible by optical excitation $E_0 + E_g$, scaled by the hopping matrix element t and plotted versus the scaled Coulomb repulsion parameter U/t. The dotted and dashed lines indicate, respectively, the paramagnetic and ferromagnetic Hartree-Fock approximations to the ground state.

The next level of approximation beyond LDA is to include spin, allowing for ferromagnetic or antiferromagnetic spin configurations. Using a perturbative approach, we estimated the magnitude of this effect for the local spin density approximation (LSDA) represented by the Perdew-Wang functional[20] and for the generalized gradient approximation (PBE)[29] and found it to be negligible. Meanwhile, there is accumulating evidence of systematic errors in density functional treatments of narrow band materials. One of the causes of these errors is the fact that the energy functional includes the Coulomb interaction of each electron with itself which is not effectively canceled by most exchange-correlation functional forms. This so-called self-interaction error has been addressed in several references such as 30–32, to name a few. Efforts are currently underway to correct this error by constructing new functionals.[33] In order to examine the self-interaction problem and the failure of the LDA approach more generally, we were motivated to consider these materials from the point of view of quantum chemical and Hubbard model analyses. For this, we focus on re-analyzing the states near the Fermi level of the ϵ and ζ materials.

IV. HUBBARD MODEL ANALYSIS

A. Infinite one-dimensional crystal

In its simplest form, the Hubbard model[35] is a two parameter representation of the basic interactions which control our many-electron system. Because of its relative mathematical accessibility and its rich physics, this model has received enormous attention – more than 7000 papers on the Hubbard model published in the last 30 years.

It is assumed that it is possible to find a basis of orthogonal single particle states, $\phi_n(\mathbf{r})\chi_\sigma$ spatially localized at each site of the lattice n and having spin $\sigma(\uparrow,\downarrow)$. In our case, we expect the spatial form of $|\phi_n(\mathbf{r})|^2$ to roughly correspond to the charge density plots shown in Fig. 7, for the n^{th} BEDT-TTF$^+$ molecular ion. The localized basis is used to construct creation ($a^\dagger_{n\sigma}$) and annihilation ($a_{n\sigma}$) operators. The Hubbard Hamiltonian can then be written

$$\mathcal{H}(t,U) = -t\sum_{n\sigma}\sum_{(n')} a^\dagger_{n\sigma}a_{n'\sigma} + U\sum_n a^\dagger_{n\uparrow}a_{n\uparrow}a^\dagger_{n\downarrow}a_{n\downarrow}, \quad (7)$$

where the parameters t and U represent the electron hopping and Coulomb repulsion matrix elements, respectively. The sum over n is taken over the sites of the lattice. The sum over n' is restricted to nearest neighbors of n.

There is one electron available for each ion which is known as the half-filling case. For simplicity, we focus on

the one-dimensional Hubbard model, which corresponds to assuming that t represents the nearest neighbor interaction and neglecting all other interactions. In terms of the tight-binding analysis of Section III D 2, this corresponds to choosing $t \approx M_{11}(\mathbf{c})$ and $t \approx M_{11}(\mathbf{a})$ for the ϵ and ζ structures, respectively.

The advantage of mapping our system to the half-filled one-dimensional nearest neighbor Hubbard model, is that we can make use of the exact calculations for the system which describe its non-trivial behavior. In particular, the insulating behavior of the one-dimensional Hubbard system at half-filling was established by the analysis of the exact ground state of the system by Lieb and Wu.[34] They found the ground state energy of this system to be given by the expression

$$E_0 = -4t \int_0^\infty \frac{J_0(x)\, J_1(x)\, dx}{x(1+\mathrm{e}^{xU/(2t)})}, \tag{8}$$

where $J_n(x)$ are Bessel functions of integer order, as plotted in Fig. 9 as a function of the scaled interaction parameter U/t. Also shown on this plot are the Hartree-Fock approximations to the ground state. These were analyzed by Johansson and Berggren[36] who showed that for the Hartree-Fock ground state takes the forms

$$E_0^{\mathrm{HF}} = -\frac{4}{\pi}t + \frac{1}{4}U \quad \text{or} \quad E_0^{\mathrm{HF}} = 0, \tag{9}$$

for the paramagnetic and ferromagnetic spin configurations, respectively. For values of $U/t > 16/\pi$, the ferromagnetic Hartree-Fock solution is more stable than the paramagnetic Hartree-Fock solution, but neither is close to the exact ground state for large values of U/t.

In addition to analyzing the ground state of this system, Lieb and Wu[34] showed that the band gap could be defined in terms of the difference between the energy to add an electron minus the energy to remove an electron:

$$E_g = \mu_+ - \mu_- = -4t + U + 8t \int_0^\infty \frac{J_1(x)\, dx}{x(1+\mathrm{e}^{xU/(2t)})} \tag{10}$$

$$= \frac{16t^2}{U} \int_1^\infty \frac{\sqrt{x^2-1}\, dx}{\sinh(2\pi t x/U)}. \tag{11}$$

The second form of the integral was derived by Ovchinnikov.[37] These analytic expressions show that $E_g > 0$ for all $U/t > 0$. In this sense, the half-filled one-dimensional Hubbard model represents an insulator for all $U/t > 0$. The magnitude of the band gap is plotted in Fig. 9 relative to the exact ground state energy E_0.

This many-body definition of E_g is substantially different from that expected from a single particle point of view. In fact, the many-body density of states would show a continuum of states above the ground state accessible by magnetic fluctuation.[37–39] More recently, the response of the half-filled one-dimensional Hubbard system to a static and time-dependent electric field has been examined in terms of a current operator.[40–42] In this work, it has been numerically established that the Mott energy gap E_g also corresponds to the threshold for optical excitations and that the static conductivity of this system also vanishes for the same form of the current operator.

For ζ-BEDT-TTF·PF_6 a band gap of $E_g \approx 0.5$ or 0.6 eV was inferred[3] from the temperature dependence of the static conductivity and the threshold for optical electric transitions. This seems to be qualitatively consistent with these results for the half-filled one-dimensional Hubbard model.

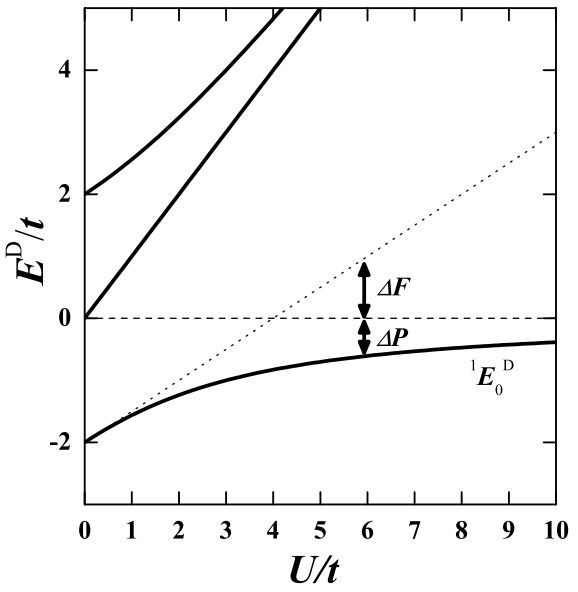

FIG. 10: Plot of the 2-electron eigenstates of the Hubbard dimer. Singlet eigenstates are indicated with bold lines. Triplet eigenstates which coincide with the triplet Hartree-Fock states are indicated with a dashed line, while the singlet Hartree-Fock ground state is indicated with a dotted line. The energies are scaled by the hopping parameter t and plotted versus the scaled Coulomb repulsion parameter U/t. The parameters ΔF and ΔP are explained in the text.

B. Dimer

In order to examine the Hubbard system in more detail, we consider a dimer system consisting of two sites and two electrons. The Hubbard model for this case can be solved exactly as detailed in the Appendix. The Hubbard model eigenvalues are graphed in Fig. 10 with the ground state having the singlet spin configuration and the energy is given by

$${}^1E_0^D = \frac{1}{2}U - \frac{1}{2}\sqrt{U^2+16t^2}. \tag{12}$$

The corresponding eigenvector is given by

$$ {}^1\Psi_0^D = \frac{1}{\sqrt{2+x^2}}(|1\rangle + |2\rangle + x|3\rangle), \tag{13} $$

where

$$ x \equiv x(U/t) = \frac{1}{2\sqrt{2}}\left(U/t + \sqrt{(U/t)^2+16}\right). \tag{14} $$

The basis states $|1\rangle$ and $|2\rangle$ correspond to 2 electrons on a site ("ionic" contributions) and state $|3\rangle$ corresponds to a valence-bond contribution[43] as defined in the Appendix.

In comparison, the corresponding dimer Hartree-Fock solutions have triplet states which are identical to those of the exact solutions, ${}^3E_0^{\rm D} = {}^3E_0^{\rm DHF} = 0$ while the lowest dimer Hartree-Fock singlet state has the energy

$$ {}^1E_0^{\rm DHF} = -2t + \frac{1}{2}U, \tag{15} $$

with the corresponding trial wavefunction having the same form as Eq. (13) with $x(U/t \equiv 0) = \sqrt{2}$. For comparison, the Hartree-Fock energy is included in the energy diagram of Fig. (10). Here it is evident that for this dimer model, the singlet Hartree-Fock solution has lower energy for values of $U/t < 4$, while the triplet Hartree-Fock solution has lower energy for $U/t > 4$. Except for $U/t << 4$, the exact ground state energy of the model is substantially lower than either Hartree-Fock approximate.

The basic physics shown here is reminiscent of the valence-bond versus molecular-orbital descriptions of the electronic structure of a H_2 molecule.[44] In describing the single ground state of the Hubbard dimer, the relative weights of the "ionic" contributions to the wavefunction represented by states $|1\rangle$ and $|2\rangle$ (Eq. A.1 and A.2) and the "valence bond" contribution represented by state $|3\rangle$ Eq. A.3) are sensitive functions of U/t through the function $x(U/t)$. From the form of the dimer eigenstate of Eq. (13), we can define the weight of the valence bond contributions to be

$$ w_{\rm vb} \equiv \frac{x^2}{2+x^2}, \tag{16} $$

and the weight of the ionic contributions to be

$$ w_{\rm ion} \equiv \frac{2}{2+x^2}. \tag{17} $$

These are plotted versus U/t in Fig. 11 where we also show the corresponding quantities for the Hartree-Fock approximation. For the exact dimer wavefunction, $w_{\rm vb} > w_{\rm ion}$ for all $U/t > 0$, while the Hartree-Fock wavefunction has $w_{\rm vb} = w_{\rm ion} = 1/2$ throughout all values of U/t.

Another approximate analysis of the one-dimensional Hubbard model is the spin density wave (SDW) approach which forces an antiferromagnetic symmetry on the ground state wavefunction.[36] We can examine this approach for the two-electron dimer system. The details

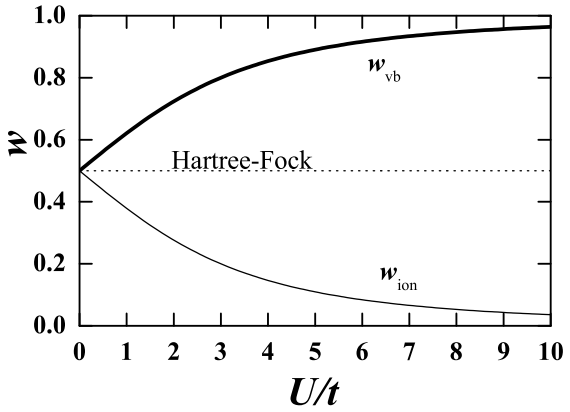

FIG. 11: Plot of the weight factors w indicating the valence-bond (bold line) and ionic (thin line) contributions to the exact ground state wavefunction of the Hubbard dimer plotted as a function the of scaled Coulomb repulsion parameter U/t. The valence-bond and ionic contributions for of the Hartree-Fock approximation are identical and are indicated with the dotted line.

are given in the Appendix. The results for the ground state energy are an improvement over the Hartree-Fock results:

$$ E_0^{\rm SDW} = \begin{cases} -2t + \frac{1}{2}U & \text{for } U/t \le 2 \\ -\frac{2t^2}{U} & \text{for } U/t > 2 \end{cases} \tag{18} $$

Here we see that for $U/t \le 2$ the Hartree-Fock solution has the lowest energy, however for $U/t > 2$, the SDW solution has lower energy than the Hartree-Fock result. However, it also turns out that for $U/t > 2$, the SDW solution includes contamination from triplet states with the weight $w_{\rm triplet} = \frac{1}{2} - \frac{t}{U}$, while the valence-bond and ionic weights are $w_{\rm vb} = \frac{1}{2}$ and $w_{\rm ion} = \frac{t}{U}$, respectively. The triplet contributions to the SDW states have the same spatial form as the valence-bond states, but have the wrong total spin.

In passing, we note that the valence-bond contribution strength $w_{\rm vb}$ is a useful parameter which characterizes the exact solution of the Hubbard dimer Hamiltonian. We can use it together with the orthogonal basis functions $\phi_1(\mathbf{r})$ and $\phi_2(\mathbf{r})$, localized on sites 1 and 2, respectively, to describe the spatial form of the electron density corresponding to the exact dimer wavefunction (Eq. 13):

$$ \rho(\mathbf{r}) = \frac{1}{2}\left(\rho_{11}(\mathbf{r}) + \rho_{22}(\mathbf{r})\right) + 2\sqrt{w_{\rm vb}(1-w_{\rm vb})}\rho_{12}(\mathbf{r}), \tag{19} $$

where

$$ \rho_{ij}(\mathbf{r}) \equiv \frac{1}{2}\left(\phi_i(\mathbf{r})\phi_j^*(\mathbf{r}) + \phi_i^*(\mathbf{r})\phi_j(\mathbf{r})\right). \tag{20} $$

In this expression we see that $w_{\rm vb}$ appears only as the product $w_{\rm vb}(1-w_{\rm vb}) = w_{\rm vb}w_{\rm ion}$. This form points

out a numerical problem for the density functional[18,19] treatment of this system. Density functional theory relies on the fact that the ground state of the system is a unique functional of the density. However, we see that for this system, the spatial form of the density is very weakly dependent on the parameter $w_{\rm vb}$ and can take the same value if $w_{\rm vb} > w_{\rm ion}$ or $w_{\rm vb} < w_{\rm ion}$ for constant $w_{\rm ion} w_{\rm vb}$. Thus, the notion of valence-bond character is virtually missing from the usual density functional treatment. López-Sandoval and Pastor[45,46] have recently developed a lattice density functional theory in which matrix elements of the one-particle density matrix, including both diagonal and off-diagonal terms, are treated variationally, which looks like a promising alternative.

V. QUANTUM CHEMICAL TREATMENT

In order to analyze this system from a different point of view, we carried out a series of calculations for monomer and dimer configurations using quantum chemical techniques.

A. Calculational details

Calculations were performed using both the CRYSTAL98[47] and Gaussian03[48] codes and using Gaussian orbital basis sets from Pacific Northwest Laboratory website.[49] After verifying that identical results could be obtained using the two codes, we focused on using the Gaussian03 code. Unless otherwise stated, the results were obtained using the 6-31G** basis set[49] and using the unrestricted spin mode. We first used the unrestricted Hartree-Fock method to optimize the atomic positions for the monomer ions BEDT-TTF$^+$ using the appropriate point group symmetry (C_{2h} for the ϵ structure and C_i for the ζ structure. The resulting C−C and C−S bond lengths are summarized in Table III and agree well with the earlier work of Demiralp and Goddard[9] and with the LDA results discussed above. The optimized structures for the neutral and charged dimers where visualized using Molden[50] and are shown in Fig 2.

We made use of several of the implementations available in the Gaussian03 code in order to broaden the comparison. In addition to Hartree-Fock (HF) calculations, we also use the Gaussian03 implementations of density functional calculations using various exchange-correlation functionals including the local spin density approximation (LSDA),[51] a generalized gradient approximation (PBE),[52] and a hybrid functional (B3LYP).[53–57]

B. Dimer calculations

In order to make a connection with the BEDT-TTF·PF_6 crystals, and with Hubbard model dimer analysis, we consider dimers of BEDT-TTF$^+$ in their nearest neighbor configurations of the crystals. This is similar to approach taken by Fortunelli and Painelli[12–14] in their analysis of other BEDT-TTF materials. The relevant dimers, $(\text{BEDT-TTF})_2^{+2}$ are not stable by themselves due to their mutual Coulomb repulsion, however we expect that comparisons of energy differences between singlet and triplet configurations in a given geometric configuration will be meaningful. Calculations on neutral dimers of $(\text{BEDT-TTF}\cdot PF_6)_2$ gave qualitatively similar results.

TABLE VII: Summary of results for dimers of $(\text{BEDT-TTF})_2^{+2}$ obtained using the Gaussian03 code[48] in the unrestricted spin mode. The labels "NN" and "NNN" indicate the nearest-neighbor and next-nearest-neighbor geometries, respectively, as listed in Table II. Calculated single particle energies ΔF and MP2 energies ΔP are listed in units of eV.

Dimer geometry	Single particle method	ΔF	ΔP
ζ (NN)	LSDA	-0.09	
	PBE	-0.05	
	B3LYP	0.24	
	HF	1.85	-0.70
ζ (NNN)	HF	2.06	-0.67
ϵ (NN)	HF	1.73	-0.65

The results for the dimer calculations, all run with the unrestricted spin mode, with total spin $S = 0$ or $S = 1$ are summarized in Table VII. The single particle energy differences are reported in terms of $\Delta F \equiv {}^1E_0^{\rm DK} - {}^3E_0^{\rm DK}$ (where K = HF, LSDA, PBE, or B3LYP). The density functional results in the LSDA and PBE approximations show a very small spin splitting as is consistent with our *pwpaw* results presented in Section III above, with the singlet energy calculated to be more stable than the triplet. The hybrid functional "B3LYP" results also show a relatively small spin splitting, but in this case the triplet configuration is found to be more stable than the singlet.

The Hartree-Fock results all show ${}^1E_0^{\rm DHF} > {}^3E_0^{\rm DHF}$ by roughly 2 eV. If we refer to Fig. 10 and imagine that these Hartree-Fock results can be analyzed in terms of the Hubbard dimer model, we would conclude that the Hubbard parameters must be such that $U/t > 4$, such as indicated by the arrow and ΔF in the diagram. Unlike the density functional calculations which underestimate the spin interactions due to the contamination of electron self-interaction, the failure of the Hartree-Fock approach is due to the overestimation of the ionic versus valence-bond configurations in the wavefunctions as shown in Fig. 11.

In order to estimate the next level of approximation beyond Hartree-Fock theory, we used a MP2 correction, which is a second order perturbation theory expansion of the spin unrestricted Hartree-Fock ground state developed by Møller and Plesset[58] and others[59,60] and available in the Gaussian03 code. The results are also presented in Table VII in terms of $\Delta P \equiv {}^1E_0^{\rm DMP2} - {}^3E_0^{\rm DMP2}$. These results show that

${}^1E_0^{\rm DMP2} < {}^3E_0^{\rm DMP2}$, so that the corrected energies now have a ordering which is consistent with the exact Hubbard dimer energies as indicated by the arrow and ΔP in Fig. 10. While it is difficult to check these results with larger basis sets, we have verified that the results are stable for smaller basis sets.

VI. CONCLUSIONS

A. Estimation of the Hubbard model parameters

The Hubbard model for the infinite chain offers a qualitative explanation of the experimental results and the Hubbard dimer model offers a plausible analysis of the failures of the density functional and Hartree-Fock calculations. We now address the question of whether or not the Hubbard model is accurate enough to be quantitative. From the point of view of matching the experimental estimate of the band gap E_g to the model, we can make the following estimate for the hopping parameter t and the Coulomb repulsion parameter U. We suppose that $t \approx 0.24$ eV as determined in the tight binding fit quoted in Table VI and take the experimental band gap to be $E_g \approx 0.5 - 0.6$ eV. This means that $E_g/t \approx 2.0 - 2.5$. From the numerical value of E_g/t, we can then infer the $U/t \approx 5 - 6$ and that $U \approx 1.2 - 1.4$ eV, which is a reasonable result.

From the comparison of the Hubbard dimer with quantum chemical results of the corresponding system, we can estimate the parameters in a different way. We suppose that the MP2 results correspond to the exact dimer ground state expressed in Eq. (12), setting $\Delta P = {}^1E_0^D - {}^3E_0^D = {}^1E_0^D$. We also suppose that the Hartree-Fock energies correspond with Eq. ((15), setting $\Delta F = {}^1E_0^{\rm DHF} - {}^3E_0^{\rm DHF} = {}^1E_0^{\rm DHF}$. We now can solve for t and U, finding $t \approx 1$ eV and $U \approx 8$ eV for all of the cases considered. This estimate for t is clearly too large, indicating that the analysis, while qualitatively correct is not quantitatively correct. Thus, while the MP2 results are able to correctly predict that the ground state is a singlet state for this system, it is not close enough to the exact result to give quantitative estimates of the Hubbard parameters. Since the MP2 corrections to the Hartree-Fock energies are approximately 190 eV, it is not perhaps surprising that further corrections are needed.

B. Outlook

This work has given us some insight into the physics of some of the simplest examples of organic charge-transfer crystals having the stoichiometry of BEDT-TTF·PF_6. We have determined that the ζ structure is energetically favored over the ϵ form, largely due to the greater stability of the corresponding lower symmetry molecular form. The ground state properties of these materials, including their bond lengths, the single particle density of states, the charge density associated with states near the Fermi level are well represented by are LDA and quantum chemical models. In order to understand the conductivity, optical, and magnetic properties of these materials, however, many body effects must be included. For example, the band gap deduced from the experimental measurements on ζ-BEDT-TTF·PF_6 from the temperature dependence of the direct current conductivity and the optical band gap[3] are consistent with the Mott-Hubbard band gap calculated for the half-filled one-dimensional Hubbard model using reasonable values for the t and U parameters.

The analysis of this system has also offered insight into the challenges of numerical treatment of many-electron interactions in narrow band materials more generally. In these systems, spin fluctuations are important. However, within density functional theory, we find that the LSDA and PBE exchange-correlation results systematically underestimate the spin fluctuations perhaps due to the contamination by the electron self-interaction. In a Hartree-Fock treatment, the self-interaction problem is removed, however by definition, correlation effects are also not treated. We analyzed the problem in more detail using a Hubbard dimer model, finding that an important component of this analysis is the inclusion of more valence-bond than ionic character in the ground state wavefunction. The Hartree-Fock treatment includes too much ionic character which destabilizes the result. A SDW treatment reduces the ionic character, but also contaminates the wavefunction with terms having the incorrect total spin. We have also shown that the one-electron density and therefore the density functional approach in its usual form is nearly blind to the valence-bond content of the wavefunction.

We have shown that the inclusion of correlation effects to correct the Hartree-Fock treatment, even at the minimal level of MP2 theory, produced qualitatively accurate results for the dimer configurations. Clearly, inclusion of higher levels of correlation are necessary for quantitative analysis of the dimer as well as the crystalline systems. There have been a number of powerful methods developed to treat highly correlated electron systems, such as the density-matrix renormalization-group (DMRG) method[61], the dynamical mean field theory (DMFT) approach[62], and quantum Monte Carlo methods.[63] While the DMRG and DMFT methods have largely focused on solving model Hamiltonian systems, LDA+U methods[32] and LDA+DMFT methods[62] are being developed in order to augment density functional treatments with correlation effects. From our analysis in the current work, we would anticipate that the LDA+U approach, which adds a Hubbard-like Coulomb term into the effective Hamiltonian and evaluates it in a mean-field approximation, would not be suitable for the BEDT-TTF·PF_6 system. From our unrestricted Hartree-Fock calculations on the $(\text{BEDT-TTF}^+)_2$ dimers, we find the energy of the singlet spin configuration to be significantly higher in energy than that of the triplet spin state, suggesting

that the mean-field treatment of this system with the LDA+U method would also give incorrect results. We hope that the analysis presented here will inspire the development of additional methods for analyzing the interesting physics of narrow band materials.

Appendix:

Here we give the details of the exact eigenstates of the Hubbard model (7) for a 2 site and 2 electron dimer system. This analysis has appeared in the literature.[64,65] There are 6 eigenstates of the Hubbard dimer. Three if them have triplet spin states and have eigenenergies of 0. The other three states are single spin states which can be represented by the following two electron basis functions:

$$|1\rangle \equiv |a^\dagger_{1\uparrow} a^\dagger_{1\downarrow}|0\rangle, \tag{A.1}$$

$$|2\rangle \equiv |a^\dagger_{2\uparrow} a^\dagger_{2\downarrow}|0\rangle \tag{A.2}$$

$$|3\rangle \equiv \sqrt{\frac{1}{2}}\left(|a^\dagger_{1\uparrow} a^\dagger_{2\downarrow}|0\rangle - |a^\dagger_{1\downarrow} a^\dagger_{2\uparrow}|0\rangle\right). \tag{A.3}$$

Here, the ket vector $|0\rangle$ represents the vacuum state. In this basis, the Hamiltonian (7) takes the form:

$$\mathcal{H} = \begin{pmatrix} U & 0 & -\sqrt{2}t \\ 0 & U & -\sqrt{2}t \\ -\sqrt{2}t & -\sqrt{2}t & 0 \end{pmatrix}. \tag{A.4}$$

We also give some of the details of the SDW solution of the 2site and 2 electron Hubbard dimer, following the approach of Johansson and Berggren.[36] The ground state wave is assumed to take the form:

$$\Psi_0^{\mathrm{SDW}} = \alpha_0 \alpha_1 |0\rangle, \tag{A.5}$$

where

$$\alpha_0 \equiv \frac{1}{\sqrt{2}}\left(\cos\theta_0 (a^\dagger_{1\uparrow} + a^\dagger_{2\uparrow}) + \sin\theta_0 (a^\dagger_{1\downarrow} - a^\dagger_{2\downarrow})\right) \tag{A.6}$$

and

$$\alpha_1 \equiv \frac{1}{\sqrt{2}}\left(\cos\theta_1 (a^\dagger_{1\uparrow} - a^\dagger_{2\uparrow}) + \sin\theta_1 (a^\dagger_{1\downarrow} + a^\dagger_{2\downarrow})\right). \tag{A.7}$$

The parameters θ_0 and θ_1 are determined variationally by minimizing the expectation value of the Hamiltonian. We find that for $U/t \leq 2$, the Hartree-Fock solution corresponding to $\theta_0 = 0$ and $\theta_1 = \pi/2$ has the lowest energy, while for $U/t > 2$, $\cos(2\theta_0) = 2t/U$ and $\theta_1 = \pi/2 - \theta_0$.

Acknowledgments

This work was supported by NSF grants No. DMR-9706575 and DMR-0405456, a SUR grant from IBM, and by Wake Forest University's DEAC high performance computing facility. We are grateful for helpful interactions with William C. Kerr, William B. Hodge, James E. Gubernatis and M. H. Whangbo.

* (Corresponding author) natalie@wfu.edu; http://www.wfu.edu/~natalie

[1] X. Bu, I. Csiarova, and P. Coppens, Acta Cryst. **C48**, 1558 (1992).
[2] X. Bu, I. Csiarova, and P. Coppens, Acta Cryst. **C48**, 1562 (1992).
[3] H.-L. Liu, L.-K. Chou, K. A. Abboud, B. H. Ward, F. E. Fanucci, G. E. Granroth, E. Canadell, M. W. Meisel, D. R. Talham, and D. B. Tanner, Chem. Mater. **9**, 1865 (1997).
[4] J. M. Williams, J. R. Ferraro, R. J. Thorn, K. D. Carlson, U. Geiser, H. H. Wang, A. M. Kini, and M.-H. Whangbo, *Organic Superconductors* (Prentice Hall, 1992).
[5] T. Ishiguro, K. Hamaji, and G. Saito, *Organic Superconductors, Second Edition* (Springer, 1998).
[6] J. Wosnitza, Current Opinion in Solid State and Materials Science **5**, 131 (2001).
[7] Y.-N. Xu, W. Y. Ching, Y. C. Jean, and Y. Lou, Phys. Rev. B **52**, 12946 (1995).
[8] W. Y. Ching, Y.-N. Xu, Y. C. Jean, and Y. Lou, Phys. Rev. B **55**, 2780 (1997).
[9] E. Demiralp and William A. Goddard III, J. Phys. Chem. **98**, 9781 (1994).
[10] E. Demiralp and William A. Goddard III, Phys. Rev. B **56**, 11907 (1997).
[11] R. Liu, X. Zhou, and H. Kasmai, Spectrochimica Acta Part A **53**, 1241 (1997).
[12] A. Fortunelli and A. Painelli, Journal of Chemical Physics **106**, 8041 (1997).
[13] A. Fortunelli and A. Painelli, Journal of Chemical Physics **106**, 8051 (1997).
[14] A. Fortunelli and A. Painelli, Phys. Rev. B **55**, 16088 (1997).
[15] J. M. Williams, H. H. Wang, T. J. Emge, U. Geiser, M. A. Beno, P. C. W. Leung, K. D. Carlson, R. J. Thorn, A. J. Schultz, and M. H. Whangbo, in *Prog. Inorg. Chem.*, edited by S. J. Lippard (John Wiley and Sons, 1987), vol. 35, p. 51.
[16] The molecule shown in Fig. 1 is from the ϵ structure. The ζ and δ forms have twisted C9-C10 and C7-C8 bonds.
[17] T. Mori, Bull. Chem. Soc. Jpn. **71**, 2509 (1998).
[18] P. Hohenberg and W. Kohn, Physical Review **136**, B864 (1964).
[19] W. Kohn and L. J. Sham, Physical Review **140**, A1133 (1965).
[20] J. P. Perdew and Y. Wang, Phys. Rev. B **45**, 13244 (1992).
[21] P. E. Blöchl, Phys. Rev. B **50**, 17953 (1994).
[22] A. R. Tackett, N. A. W. Holzwarth, and G. E. Matthews, Computer Physics Communications **135**, 348 (2001), available from the website http://pwpaw.wfu.edu.
[23] N. A. W. Holzwarth, A. R. Tackett, and G. E. Matthews,

Computer Physics Communications **135**, 329 (2001), available from the website http://pwpaw.wfu.edu.

[24] (1999), openDX is an open source visualization project based on IBM's Data Explorer software and available from the web site http://www.opendx.org.

[25] C. L. Fu and K. M. Ho, Phys. Rev. B **28**, 5480 (1983).

[26] Y. B. Abraham, N. A. W. Holzwarth, R. T. Williams, G. E. Matthews, and A. R. Tackett, Phys. Rev. B **64**, 245109 (2001).

[27] G. Gilat and L. J. Raubenheimer, Physical Review **144**, 390 (1966).

[28] G. Gilat and Z. Kam, Phys. Rev. Lett. **22**, 715 (1969).

[29] J. P. Perdew, K. Burke, and M. Ernzerhof, Phys. Rev. Lett. **78**, 1396 (1997).

[30] J. P. Perdew and A. Zunger, Phys. Rev. B **23**, 5048 (1981).

[31] D. Vogel, P. Krüger, and J. Pollmann, Phys. Rev. B **54**, 5495 (1996).

[32] V. I. Anisimov, ed., *Strong Coulomb correlations in electronic structure calculations: Beyond the local density approximation* (Gordon and Breac Science Publishers, 2000).

[33] J. P. Perdew and K. Schmidt, in *Density functional theory and its application to materials, AIP Conference Proceedings*, edited by V. V. Doren, C. V. Alsenoy, and P. Geerlings (American Institute of Physics, 2001), vol. 577, pp. 1–20.

[34] E. H. Lieb and F. Y. Wu, Phys. Rev. Lett. **20**, 1445 (1968).

[35] J. Hubbard, Proceedings of the Royal Society of London, Series A **276**, 238 (1963).

[36] B. Johansson and K.-F. Berggren, Phys. Rev. **181**, 855 (1969).

[37] A. A. Ovchinnikov, Soviet Physics JETP **30**, 1160 (1970).

[38] M. Takahashi, Progress of Theoretical Physics **42**, 1098 (1969).

[39] T. Wilkens and R. M. Martin, Phys. Rev. B **63**, 235108 (2001).

[40] R. M. Fye, M. J. Martins, D. J. Scalapino, J. Wagner, and W. Hanke, Phys. Rev. B **44**, 6909 (1991).

[41] E. Jeckelmann, F. Gebhard, and F. H. L. Essler, Phys. Rev. Lett. **85**, 3910 (2000).

[42] E. Jeckelmann, Physical Review B **67**, 075106 (2003).

[43] W. Heitler and F. London, Z. Physik **44** (1927).

[44] L. Pauling and E. B. Wilson, *Introduction to Quantum Mechanics* (McCraw-Hill Book Company, Inc., 1935), chap. 43.

[45] R. López-Sandoval and G. M. Pastor, Phys. Rev. B **67**, 035115 (2003).

[46] R. López-Sandoval and G. M. Pastor, Phys. Rev. B **69**, 085101 (2004).

[47] V. R. Sanunders, R. Dovesi, C. Roetti, M. Causà, N. M. Harrison, R. Orlando, C. M. Zicovich-Wilson, **CRYSTAL98** User's Manual, University of Torino, Torino, 1998.

[48] Gaussian 03, Revision C.1, M. J. Frisch, G. W. Trucks, H. B. Schlegel, G. E. Scuseria, M. A. Robb, J. R. Cheeseman, J. A. Montgomery, Jr., T. Vreven, K. N. Kudin, J. C. Burant, J. M. Millam, S. S. Iyengar, J. Tomasi, V. Barone, B. Mennucci, M. Cossi, G. Scalmani, N. Rega, G. A. Petersson, H. Nakatsuji, M. Hada, M. Ehara, K. Toyota, R. Fukuda, J. Hasegawa, M. Ishida, T. Nakajima, Y. Honda, O. Kitao, H. Nakai, M. Klene, X. Li, J. E. Knox, H. P. Hratchian, J. B. Cross, C. Adamo, J. Jaramillo, R. Gomperts, R. E. Stratmann, O. Yazyev, A. J. Austin, R. Cammi, C. Pomelli, J. W. Ochterski, P. Y. Ayala, K. Morokuma, G. A. Voth, P. Salvador, J. J. Dannenberg, V. G. Zakrzewski, S. Dapprich, A. D. Daniels, M. C. Strain, O. Farkas, D. K. Malick, A. D. Rabuck, K. Raghavachari, J. B. Foresman, J. V. Ortiz, Q. Cui, A. G. Baboul, S. Clifford, J. Cioslowski, B. B. Stefanov, G. Liu, A. Liashenko, P. Piskorz, I. Komaromi, R. L. Martin, D. J. Fox, T. Keith, M. A. Al-Laham, C. Y. Peng, A. Nanayakkara, M. Challacombe, P. M. W. Gill, B. Johnson, W. Chen, M. W. Wong, C. Gonzalez, and J. A. Pople, Gaussian, Inc., Pittsburgh PA, 2003.

[49] Basis sets were obtained from the Extensible Computational Chemistry Environment Basis Set Database, Version 02/25/04, as developed and distributed by the Molecular Science Computing Facility, Environmental and Molecular Sciences Laboratory which is part of the Pacific Northwest Laboratory, P.O. Box 999, Richland, Washington 99352, USA, and funded by the U.S. Department of Energy. The Pacific Northwest Laboratory is a multi-program laboratory operated by Battelle Memorial Institute for the U.S. Department of Energy under contract DE-AC06-76RLO 1830. Contact David Feller or Karen Schuchardt for further information.

[50] G.Schaftenaar and J. Noordik, J. Comput.-Aided Mol. Design **14**, 123 (2000).

[51] S. H. Vosko, L. Wilk, and M. Nusair, Can. J. Phys. **58**, 1200 (1980).

[52] J. P. Perdew, K. Burke, and M. Ernzerhof, Phys. Rev. Lett. **77**, 3865 (1996), erratum – Phys. Rev. Let. **78**, 1396 (1997).

[53] C. Lee, W. Yang, and R. G. Parr, Phys. Rev. B **37**, 785 (1988).

[54] A. D. Becke, J. Chem. Phys. **88**, 1053 (1988).

[55] B. Miehlich, A. Savin, H. Stoll, and H. Preuss, Chem. Phys. Lett. **157**, 200 (1989).

[56] A. D. Becke, J. Chem. Phys. **98**, 5648 (1993).

[57] P. J. Stephens, F. J. Devlin, C. F. Chabalowski, and M. J. Frisch, J. Phys. Chem. **98**, 11623 (1994).

[58] C. Møller and M. S. Plesset, Phys. Rev. **46**, 618 (1934).

[59] M. Head-Gordon and J. A. Pople, Chemical Physics Letters **153**, 503 (1988).

[60] M. J. Frisch, M. Head-Gordon, and J. A. Pople, Chemical Physics Letters **166**, 275 (1990).

[61] E. Jeckelmann, Phys. Rev. B **66**, 045114 (2002).

[62] S. Y. Savrasov, A. Toropova, M. I. Katsnelson, A. I. Lichtenstein, V. Antropov, and G. Kotliar, *Electronic structure and magnetic properties of solids* (2004), arXiv:cond-mat/0409703v1.

[63] W. M. C. Foulkes, L. Mitas, R. J. Needs, and G. Rajagopal, Reviews of Modern Physics **73**, 33 (2001).

[64] A. B. Harris and R. V. Lange, Phys. Rev. **157**, 295 (1967).

[65] M. J. Rice, Solid State communications **31**, 93 (1979).